POLITECNICO
MILANO 1863

SCUOLA DI INGEGNERIA INDUSTRIALE
E DELL'INFORMAZIONE

Executive Summary of the Thesis

Carbon-fiber/PEKK composite: mode I static and fatigue analysis

Laurea Magistrale in Space Engineering - Ingegneria spaziale

Author: Pietro Gazzi

Advisor: Prof. Antonio Mattia Grande

Co-advisor: Dott. Enrico Chemello

Academic year: 2021-2022

1. Introduction

In this thesis, it will be presented a study concerning the numerical and experimental characterization of APC(PEKK-FC)/S2 laminates produced with a hot-press process. This material has been commercially available since 2017 and has not been characterized thoroughly. In particular, a numerical optimization process has been developed to determine the fracture toughness of uni-directional laminates in a static environment and a study regarding its fatigue response.

2. Experimental campaign

The double cantilever beam is the most used experimental method to evaluate the mode I fracture toughness. In this particular case, it is used to study the interlaminar fracture toughness of a unidirectional laminate. The experimental setup exploited is coherent with the ASTM standard [1]. The laminate is produced with a pre-crack obtained with an insert placed between the two middle plies. The two external faces of the laminate are attached through hinges to the tensile test machine.
During the mode I traction the fiber-bridging phenomena occurred as visible in Figure 1, this experimental artifact modifies the response of

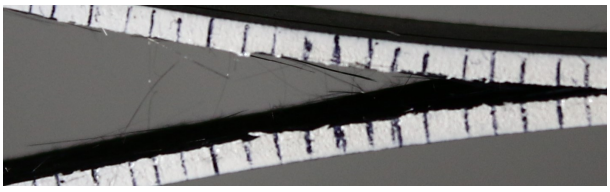

Figure 1: Fiber bridging

the specimen and drastically changes the properties of the material. Fiber bridging has historically been ascribed to next-layer fiber nesting and weak interfaces. As data reduction method is used the *modified beam theory* [7]. The expression of the energy release rate for this method is reported in Equation 1.

$$G_{MBT} = \frac{3P\delta}{2ba} \tag{1}$$

Where P is the load applied, δ is the displacement at the load point, a is the crack opening, and b is the specimen width. This is one of the most conservative methods that overestimate fracture toughness.
The result of this computation on 4 different specimens is reviewed in Figure 2. Fiber-bridging induces an alteration of the fracture toughness during the experiment. In fact, it enhances the mechanical properties of the laminate. The fracture toughness increases during

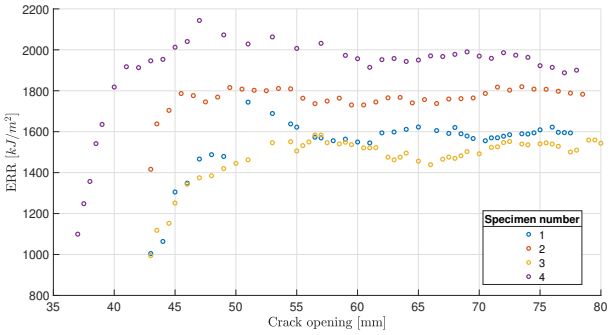

Figure 2: Mixed beam theory energy release rate

the crack growth, and it arrives at a constant value when the process zone is fully developed. A mode I fatigue test has also been performed, the configuration of the test is the same as previously mentioned, however, a cyclic displacement is applied instead of a quasi-static one. The test result can be resumed with the Paris law, which links the fracture toughness to the crack speed propagation as in Equation 2 as Schon [8].

$$\frac{\mathrm{d}a}{\mathrm{d}N} = C(G_{max})^m \tag{2}$$

Where da/dN is the crack speed, G_{max} is the maximum fracture toughness of the cycle, and C and m are fitting parameters. The experimental result and the fitting law are represented in Figure 3, while the fitting parameters found are reported in Table 1.

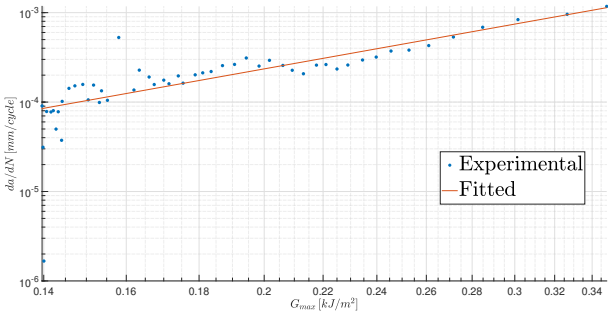

Figure 3: Experimental fatigue law fitting

$C\,[m^3/kJ]$	$m\,[-]$
0.0229	2.8438

Table 1: Paris law fitted parameters.

3. Static FEM analysis

Simulations are an important element of this characterization because they reduce the need for time-consuming and expensive experimental studies. In this study, it is presented the Finite element analysis of the DCB test. Various numerical techniques can be employed for this crack development study, such as the Virtual crack closure technique (VCCT) or extended FEM (XFEM). The crack propagation is modeled with Cohesive elements (CZM). CZM, first introduced by Hillerborg [4], in the fracture mechanics context, is based on the presence of a layer of particular elements, where the crack will grow, endowed with a traction separation law. The most common cohesive law is the bilinear one, which has a linear elastic part and a linear degradation. Due to the occurrence of the fiber-bridging phenomena and the strong increase of fracture toughness during the test, the most common law is not suitable. An alternative can be the tri-linear one, such as the one proposed by Davila [2]. In order to achieve a numerical representation most compliant with the test, it is selected the tri-linear model of Gong [3], in which the peaks of the two super-imposed cohesive elements do not coincide. The traction response, depending on the separation of the element is described as Equation 3.

$$t = (1 - D_S)K_0\delta \tag{3}$$

Where t is the traction, D_S is the degradation of the element, K_0 is the slope of the elastic part and δ is the separation of the element. The damage function is formalized as a piece-wise defined function, characterized in each part by a slope. The damage function is written in Equation 4.

$$D_S = \begin{cases} 0 & \delta \leq \delta_0 \\ \left(1 - \dfrac{K_{\mathrm{AB}}}{K_0}\right)\left(1 - \dfrac{\delta_0}{\delta}\right) & \delta_0 < \delta \leq \delta_{\mathrm{f_1}} \\ 1 - \dfrac{K_{\mathrm{BC}}}{K_0}\left(1 - \dfrac{\delta_{\mathrm{f}}}{\delta}\right) & \delta_{\mathrm{f_1}} < \delta \leq \delta_{\mathrm{f}} \\ 1 & \delta > \delta_{\mathrm{f}} \end{cases} \tag{4}$$

The slopes of the law used in the previous formulation are expressed in Equation 5.

$$\begin{cases} K_{0A} = K_1 + K_2 \\ K_{AB} = \dfrac{t_b - (t_0 + K_2\delta_0)}{t_{fb} - t_0} \\ K_{BC} = \dfrac{t_b}{\delta_{f_1} - \delta_f} \end{cases} \tag{5}$$

Parameters	Unit	Value
K_I	MPa/mm	10^4
K_{II}	MPa/mm	-
t_0	MPa	50
t_{FB}	MPa	0.7
G_{ini}	kJ/m^2	1.0
G_{SS}	kJ/m^2	1.5

Table 2: Cohesive element parameters.

The nomenclature used and the final representation of the cohesive law are presented in Figure 4 and the parameters used in Table 2.

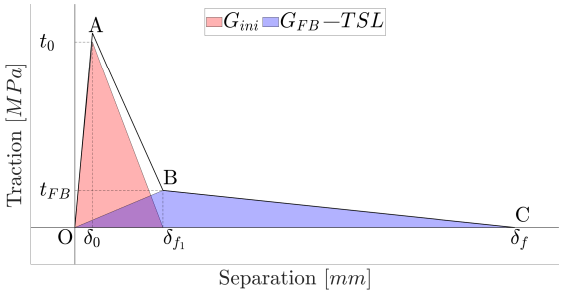

Figure 4: Tri-linear traction separation law

The delamination simulation is performed in Abaqus [9]. The commercial software is used to build the Finite Element model as presented in Figure 5. In the image, it is possible to see the modeling approach.

The traction separation law parameters are partially found in the literature such as the elastic modulus and partly retrieved from the experimental campaign such as the initial and steady-state fracture toughness. The material variables are reported in Figure 5.
Due to the presence of the fiber-bridging phenomena, the fracture process zone does not interest only the crack tip, but all the zone in which the fibers perform an active resistance to the detachment. A bi-linear cohesive, due to the low final separation of the element, is characterized by a small process zone, and it is not able to describe the process zone length. In this case, where the elements are active since a high detachment, the process zone is more representative of what is observed experimentally. The

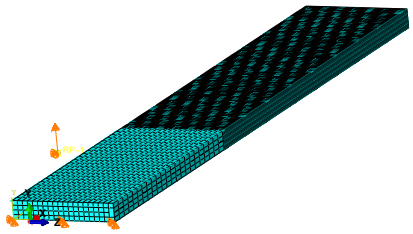

Figure 5: 3D FEM mesh and boundary conditions

process zone at the end of the simulation is reported in Figure 6.

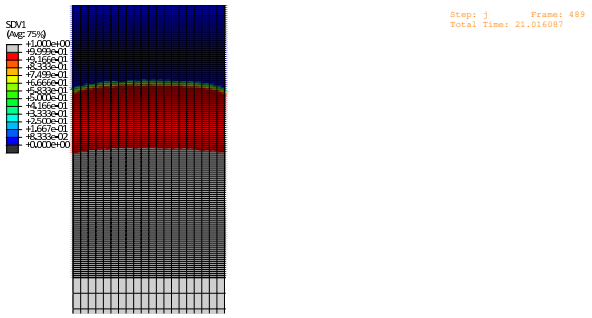

Figure 6: Element degradation end of simulation

Cohesive elements are also strictly mesh-dependent, the right decision in the mesh size is crucial to obtain an accurate result. In order to evaluate the mesh goodness of the model different models with different mesh refinement have been implemented and the results are pictured in Figure 7.

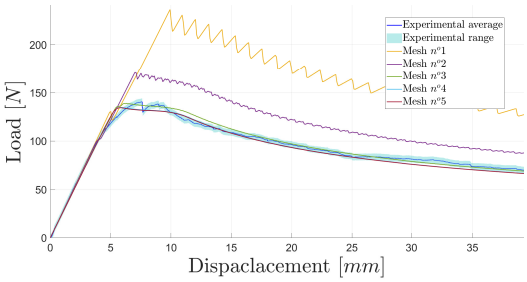

Figure 7: Load displacement curve

Coarser mesh such as the n^o1 are far from convergence result and present an aliasing effect due to the big effect induced by the total degradation of an elements' row.
The most refined mesh is used to understand

how much the element size should be small. The result of this analysis has also good compliance between the numerical model and the experimental one.

4. Parameters fitting

The further study performed in the thesis has been the development of an optimization technique to obtain a numerical response that is the best representation of the experimental one. The parameter of merit of the fit between numerical and experimental responses is the error of the load-displacement curve. The error is formalized as Equation 6, which is a global error on all the domains.

$$err = \frac{\sqrt{\sum_{i=1}^{N}\left(P_F(\delta_i) - P_e(\delta_i)\right)^2\left(\delta_i - \delta_{i-1}\right)}}{\sqrt{\sum_{i=1}^{N}\left(\delta_i - \delta_{i-1}\right)}} \quad (6)$$

Where P_F is the load experienced by the FEM model, while P_e is the experimental one.
The algorithm used is the Neldel Mead algorithm [6].
The cohesive law is based on four variables, however, the optimization is conducted with two of them considered fixed. In particular the maximum strength and the separation at which first the degradation starts are not considered variables of the problem, in fact, both of them do not reflect any properties of the material but they are selected for stability reasons and to preserve the linear part of the load-displacement curve.
The parameters of the fitting, instead, are the initial fracture toughness G_{ini} and the fiber bridging fracture toughness G_{FB}, so respectively the red and blue areas of Figure 4. The starting points of the optimization are the initial and maximum difference of fracture toughness retrieved with the modified beam theory.
Figure 8 reports the traction separation law before and after the parameter fitting.
The main effect of error minimization is the increase in the maximum separation at which the element fully degrade.
The algorithm finds a path in which the error reduction is steeper and it follows it until the reduction ends, then the second parameter optimization follows. Firstly it modified the fiber-

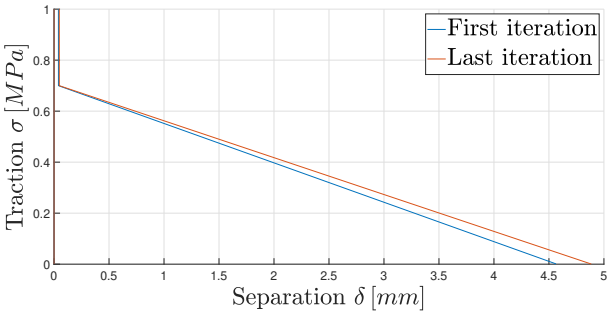

Figure 8: Tri-linear constitutive law optimization

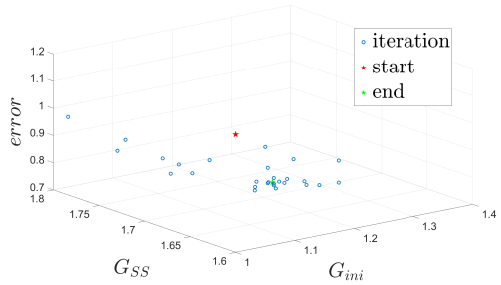

Figure 9: Tri-linear error minimization

bringing toughness because it allows a faster error decrement, this is related to the error definition.
In Table 3 the initial and final parameters of the optimization are reported. Both the parameters have increased their magnitude. Even if the beam theory overestimates the fracture toughness, the numerical approach requires higher parameters to catch the results, this shows a small discrepancy between the numerical model and the experimental one.
The fitting is also visible from the load-displacement curve reported in Figure 10.
The error is decreased by the 60% as in Table 4. The gain is significant and it allows the user to achieve the best performances of the presented model in the description of delamination.

	$G_{ini}\,[kJ/m^2]$	$G_{SS}\,[kJ/m^2]$
Initial	1.0	1.6
Final	1.24	1.70

Table 3: Tri-linear cohesive optimization parameters.

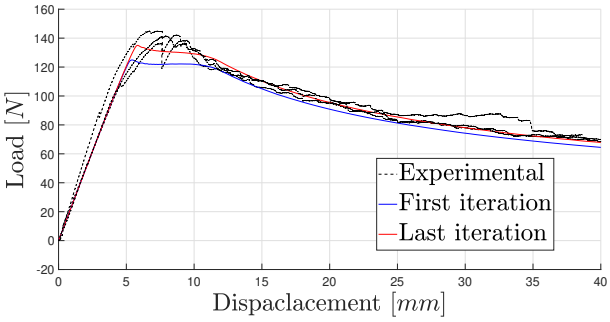

Figure 10: Tri-linear optimized load-displacement curve

Initial error	1.13
Final error	0.71

Table 4: Tri-linear cohesive optimization parameters error.

5. Fatigue modeling

Different strategies could be exploited in order to model fatigue in a cohesive study. In this case, to avoid an excessive computational load for the fatigue analysis the displacement/load is considered fixed during the fatigue step, and degradation is only simulated by the cohesive law depending on pseudo time. So instead of replicating the cyclic behavior of the test, it used only the envelope of the load such as Figure 11. The fatigue implementation is obtained by adding a fatigue degradation at the cohesive level. In the fatigue study, the degradation is composed of the summation of a static contribution and a fatigue one.

$$D = D_s + D_f \tag{7}$$

In this thesis, Kawashita's model [5], in a tri-linear fashion is used for the cohesive elements in the fatigue analysis.

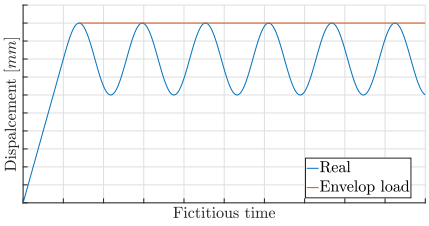

Figure 11: Numerical approach to fatigue

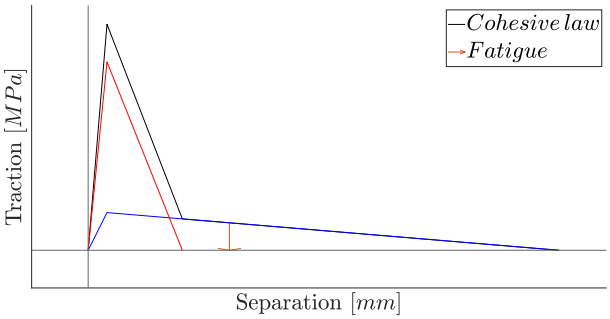

Figure 12: Fatigue tri-linear law

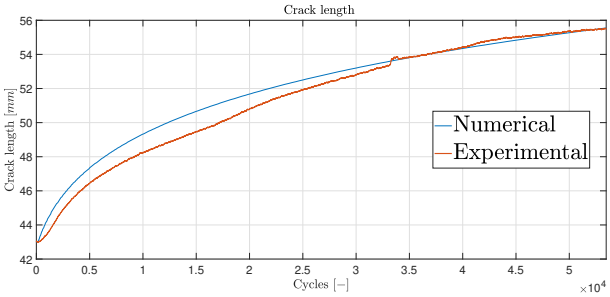

Figure 13: Crack evolution

$$\frac{\mathrm{d}D_f}{\mathrm{d}N} = \begin{cases} \frac{1-D_{s1}}{l_e}\frac{\mathrm{d}a}{\mathrm{d}N} & if\ \delta_0 \le \delta < \delta_{f1} \\ \frac{1-D_{s2}}{l_e}\frac{\mathrm{d}a}{\mathrm{d}N} & if\ \delta_{f1} \le \delta < \delta_f \end{cases} \tag{8}$$

$$D_f(N+\Delta N) \approx D_f(N) + \frac{\mathrm{d}D_f}{\mathrm{d}N} f \Delta time \tag{9}$$

Figure 12 represents the cohesive law of a single element subjected to a pre-aperture and then a fatigue step. During the static part it proceeds as in the previous analysis however once the fatigue starts, at a constant aperture, the element starts degrading without further aperture.

In Figure 13 it is pictured the comparison between the numerical and experimental curve. The latter starts with a non-propagating region of the first cycle and some spikes appear. The former presents a smooth behavior, characterized by a constant decrease of the derivative and an immediate start of the crack propagation.
The fitting of the curve is more evident in the last part, where the experimental one arrives in a stable condition and the simulation is more significant. The major discrepancy between the two curves lies in the onset of the crack propagation, in fact, the numerical model is not able to predict a quiescent part at the beginning of the experiment. The laminate experiences a nucleation period in which the crack does not evolve.

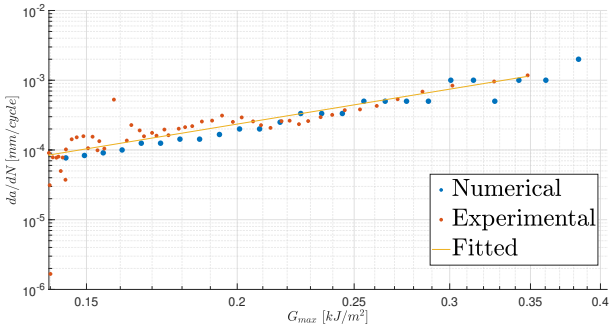

Figure 14: Paris law fatigue

Further steps shall be moved to stem this inequality. The presence of spikes or crack acceleration inhomogeneity during the test is expected, due to the presence of defects, however, the constant crack of the first cycles is common. It is probably related to the opposition of the material to the beginning of energy release.
Figure 14 shows the juxtaposition between the numerical and the experimental fatigue law. The behavior and the magnitude of the law obtained are the same for the two scatter. The compliance in this case is much more relevant with respect to the crack length. This is caused by the nature itself of the cohesive element, which is a function of the Paris law.

6. Conclusions

The study presented focused on the experimental and numerical characterization of the mode I delamination of a PEKK/carbon-fiber unidirectional laminate both in static and fatigue conditions. The use of cohesive elements is easy and highly adaptable, however, they are only suitable for problems similar to delamination. Other numerical tools can be used in a wider variety of fields, such as XFEM or phase-field. Further steps could be moved to obtain such results also with other numerical methods. The study ended with a parameter fitting for better compliance between numerical and experimental results. In recent years optimization algorithms have been used intensively in structural mechanics in order to design high-performance parts. It would be interesting to use the same procedure for the maximization of performances and not only for parameter fitting. The major lack of this study is the absence of different modes of delamination, this should be immediately the next step of the thesis.

References

[1] Standard test method for mode i interlaminar fracture toughness of unidirectional fiber-reinforced polymer matrix composites 1. 2009.

[2] Carlos G Dávila, Cheryl A Rose, and Pedro P Camanho. A procedure for superposing linear cohesive laws to represent multiple damage mechanisms in the fracture of composites. *International Journal of Fracture*, 158(2):211–223, 2009.

[3] Yu Gong, Yixin Hou, Libin Zhao, Wangchang Li, Jianyu Zhang, and Ning Hu. A modified mode i cohesive zone model for the delamination growth in dcb laminates with the effect of fiber bridging. *International Journal of Mechanical Sciences*, 176:105514, 2020.

[4] A. Hillerborg, M. Modéer, and P.-E. Petersson. Analysis of crack formation and crack growth in concrete by means of fracture mechanics and finite elements. *Cement and Concrete Research*, 6(6):773–781, 1976.

[5] Luiz F Kawashita and Stephen R Hallett. A crack tip tracking algorithm for cohesive interface element analysis of fatigue delamination propagation in composite materials. *International Journal of Solids and Structures*, 49(21):2898–2913, 2012.

[6] J. A. Nelder and R. Mead. A simplex method for function minimization. *The Computer Journal*, 7(4):308–313, 01 1965.

[7] T Kevin O'Brien. *Results of ASTM round robin testing for mode 1 interlaminar fracture toughness of composite materials*, volume 104222. National Aeronautics and Space Administration, Langley Research Center, 1992.

[8] Joakim Schön. A model of fatigue delamination in composites. *Composites Science and Technology*, 60(4):553–558, 2000.

[9] Michael Smith. *ABAQUS/Standard User's Manual, Version 6.9*. Dassault Systèmes Simulia Corp, United States, 2009.